Atom-Photon Interaction

Manuel Antoinette

January 10, 2023

In this lab we build a setup that simultaneously performs Doppler-free absorption spectroscopy on a natural Rubidium vapor chamber and allows us to observe the effects of electromagnetically indicated transparency (EIT) on it. Dopplerfree spectroscopy is a method to combat the effects of Doppler broadening, by saturating the transition of electrons that see the laser beam without a Doppler shift. EIT is a quantum interference effect in three-state systems, where one of the transitions is prohibited. Here, we work with Λ-systems, which have two ground states and one excited state. We realize this system by exposing the rubidium probe to a magnetic field and using the levels of the Zeeman splitting as our ground states. We manage to measure a detailed absorption profile of the D_1 transition of both ^{87}Rb and ^{85}Rb. From the Doppler broadened dips we calculated the atomic vapor to have had reasonable temperatures of $(72\pm6)\,^{\circ}$C and $(42\pm4)\,^{\circ}$C. For the EIT we managed to observe the peaks for three of the four ^{87}Rb D_1 transitions. For these we showed that the energy difference between the ground states of our Λ-system is given by the expected Zeeman splitting. Finally we briefly investigated the shape of the EIT peak for various detunings.

Contents

Laser Safety Notice

In this lab we work with an invisible laser beam with a maximum power of 80 mW. Even the 30 mW of power used in the experiments can severely damage the eyes. Appropriate laser safety measurements with IR-blocking goggles are required.

1 Introduction

Understanding the interaction between light and matter is of fundamental and practical interest. It opens up a manifold of possibilities to manipulate states of matter with laser beams and allows us to engineer light with particular properties by tailoring its interaction with atoms. The research field which deals with light-matter interaction is called quantum optics.

In this lab we performed Doppler-free spectroscopy and observed the effects of electromagnetically induced transparency (EIT) on Rubidium. To achieve this we built a setup using an array of mirrors, waveplates, (polarizing) beamsplitters and acousto-optical modulators (AOMs).

Dopplerfree spectroscopy or saturated absorption spectroscopy is a method to combat the effects of Doppler broadening. As the atoms in a gas move with some velocity relative to the light beam, they see the photons Doppler shifted. This significantly broadens the frequency range, at which a gas absorbs light. With Doppler-free spectroscopy we use two counter-propagating beams to gain further insight into the actual line width of an absorption line, without Doppler broadening effects.

EIT is a quantum interference effect. Here, we look at Λ-level systems (see figure (2)) and excite the ground state electrons, in such a way that their transition probability amplitudes interfere destructively. This induces a narrow transparency window around an absorption line. The position and shape of this spectral transparency peak depends on the energy level difference of the two ground state and on the excitation frequencies. This is what we investigated in this lab.

2 Theory

2.1 Level Structure of ^{87}Rb

The atom used in this experiment is Rubidium (Rb). Natural Rb has two isotopes, ^{85}Rb and ^{87}Rb. Its ground state electron configuration is

$$1\,\mathrm{s}^2 2\,\mathrm{s}^2 2\,\mathrm{p}^6 3\,\mathrm{s}^2 3\,\mathrm{p}^6 3\,\mathrm{d}^{10} 4\,\mathrm{s}^2 4\,\mathrm{p}^6 5\,\mathrm{s}^1,$$

with a single $5\,\mathrm{s}^1$ electron in the valence band. Its energy-level structure therefore resembles the one of hydrogen. In its first excited state, the single electron becomes a $5\,\mathrm{p}^1$ electron.

Due to spin-orbit coupling we get one ground state $5^2\mathrm{S}_{1/2}$ (Russell-Saunders notation[1]) and two excited states $5^2\mathrm{P}_{1/2}$ and $5^2\mathrm{P}_{3/2}$. Here we will be focusing on the D_1 transition from $5^2\mathrm{S}_{1/2}$ to $5^2\mathrm{P}_{1/2}$, which has a fine energy splitting of

$$\Delta E_{\mathrm{D}_1} = h \cdot 377.107\,463\,\mathrm{THz}.$$

Due to the magnetic dipole moment in the nucleus induced by the orbital motion of the valence electron and due to the electrostatic interaction between the valence electron and the non-vanishing electric quadrupole moment of the nucleus, we further get hyperfine splitting of the energy levels. The nuclear angular momentum $\vec{I}$ and the electron angular momentum $\vec{J}$ get coupled to the total angular momentum $\vec{F} = \vec{I} + \vec{J}$. To characterize the hyperfine structure, we use the total angular momentum quantum number F, which in the case of the $5^2\mathrm{S}_{1/2}$ and $5^2\mathrm{P}_{1/2}$ states of ^{87}Rb takes the values $F = 1$ and $F = 2$. The hyperfine structure of the D_1 transition of ^{87}Rb is displayed in figure (1).

In the presence of an external magnetic field B, the hyperfine levels split into sublevels depending on the angular distribution of the electron wave function. This is the Zeeman effect. The corresponding Zeeman splitting is given by

$$\Delta E = g_F \mu_B \Delta m_F B, \tag{1}$$

where g_F is the Lande factor, which depends on F, I and J, μ_B is the Bohr magneton and Δm_F the difference in the magnetic quantum number. Electric dipole transitions must obey the selection rules

$$\Delta F = 0, \pm 1 \text{ (not } 0 \to 0)$$
$$\Delta m_F = 0, \pm 1 \text{ (determined by light polarization)}.$$

2.2 Doppler Broadening

When performing absorption spectroscopy, the spectral width of the transmission dip is way wider than the actual line width of an absorption line. This is due to the atoms in a gas moving around with a velocity v. The laser frequency in the atoms frame of reference is therefore shifted by $\delta\nu = \nu_0 \cdot \frac{v}{c}$, where ν_0 is the laser frequency in a resting frame and c the speed of light. If we assume that the velocities in a gas of of temperature T follow a Maxwell-Boltzmann distribution centered around $v = 0$ and with a width of $\sqrt{2k_BT/m}$, where k_B is the Boltzmann constant, and m the atomic mass, we expect the absorption profile to have a frequency full-width at half-maximum amplitude (FWHM) of

$$\Delta\nu_{1/2} = \frac{\nu_0}{c}\left(\frac{8 \cdot \ln 2 \cdot k_B T}{m}\right)^{1/2}. \tag{2}$$

[1] Russell-Saunders notation: $n^{2S+1}L_J$, where n is the principal electronic quantum number, L is the orbital quantum Number indicated in spectroscopic notation (S, P, D, ...), S is the spin and J is the total angular momentum $\vec{J} = \vec{L} + \vec{S}$.

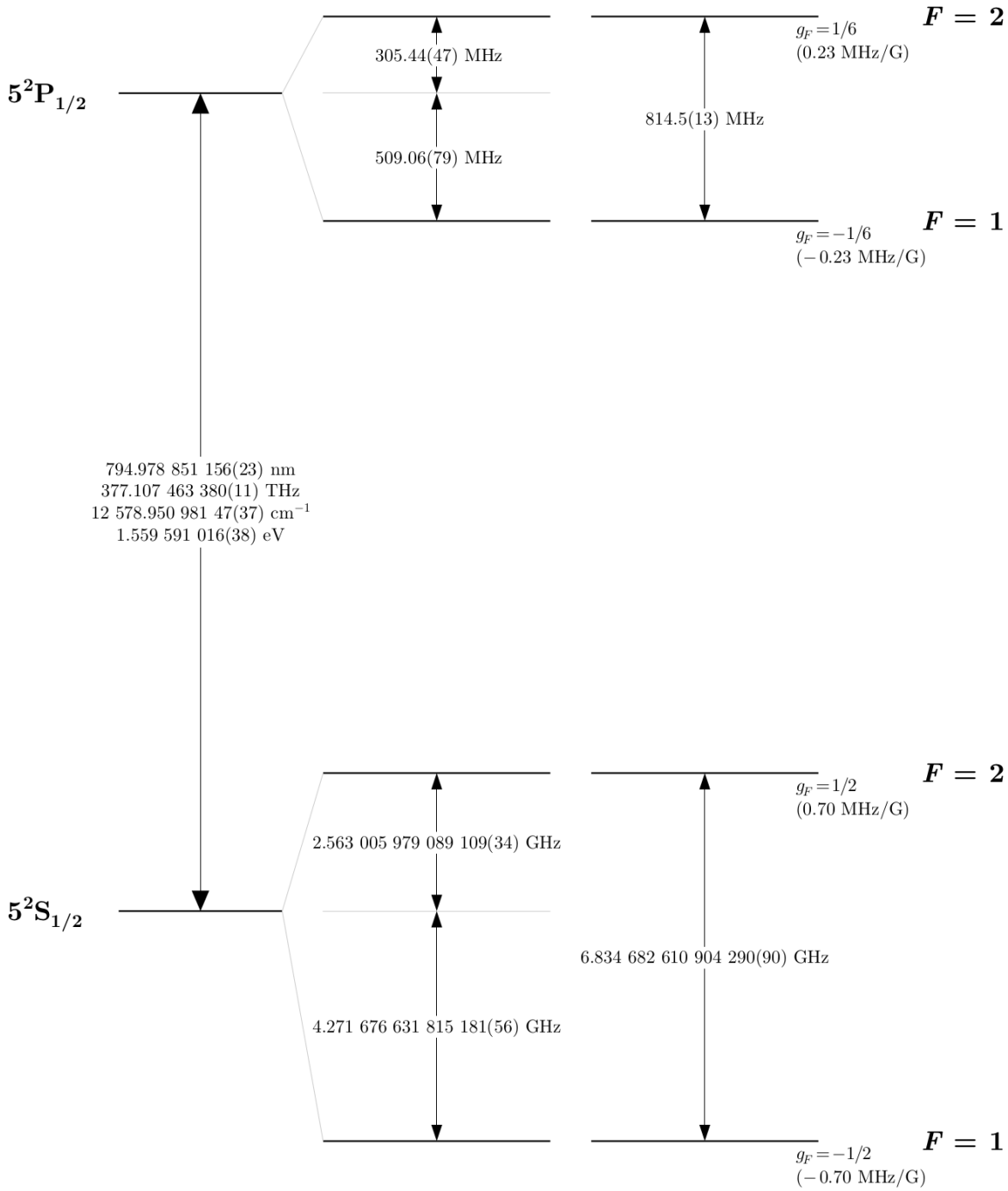

Figure 1: Fine and hyperfine structure of the D_1 transition of ^{87}Rb ($5^2S_{1/2} \rightarrow 5^2P_{1/2}$) [2].

Plugging in the values for the D_1 transition of ^{87}Rb at room temperature,

$$\nu_0 = (377.107\,463\,380 \pm 0.000\,000\,011)\,\text{THz},$$
$$T = 296.15\,\text{K},$$
$$m = (1.443\,160\,648 \pm 0.000\,000\,072) \times 10^{-25}\,\text{kg},$$

we get

$$\Delta\nu = 498.588\,\text{MHz},$$

which is two orders of magnitude larger than the Natural line width of the D_1 transition of 5.750 MHz [2].

2.3 Dopplerfree Spectroscopy

To circumvent the effects of Doppler broadening, one can use Doppler-free absorption spectroscopy. Two counter-propagating continuous wave beams of the same frequency called pump and probe beam are sent through the atomic vapor, and we only measure the intensity of the probe beam. The role of the pump beam is to saturate the optical transition. If the laser frequency is set to the transition frequency $\nu = \nu_0$, both the probe and the pump beam address the same atoms, namely those with $v = 0$ (along the beams propagation direction). Therefore, the probe beam is absorbed less, and we see a spike in the transmission. If the laser frequency is not tuned to the transition frequency though, $\nu \neq \nu_0$, the probe and pump beam each target different atoms, one those with $v = +\delta v$ and the other those with $v = -\delta v$. The probe beam is therefore fully absorbed, according to the Doppler broadening.

For multi-level atoms we will see a peak in the transmission for every transition line. If these are within a single Doppler-broadened feature, we will also see an additional peak at a frequency exactly between two transitions. This is called crossover resonance and is the result of moving atoms seeing the pump and probe beams resonant with two separate transitions.

2.4 Electromagnetically Induced Transparency

EIT occurs in three state systems. Here, we will work with Λ-systems with two ground states $|g_1\rangle$, $|g_2\rangle$ and one excited state $|e\rangle$, as shown in figure (2). We then drive the transitions $|g_1\rangle \to |e\rangle$ and $|g_2\rangle \to |e\rangle$ with a probe beam of frequency ν_p and a control beam with frequency ν_c respectively. We are only interested in the transmission intensity of the probe beam. Now, if the two beam frequencies match their respective transition frequencies, so $\nu_p = \nu_{e,g_1}$ and $\nu_c = \nu_{e,g_2}$, the atoms in the ground states $|g_1\rangle$ and $|g_2\rangle$ are being excited to the state $|e\rangle$. But, the probability amplitudes for the two transitions $|g_1\rangle \to |e\rangle$ and $|g_2\rangle \to |e\rangle$ interfere destructively, so the transition $|g_1\rangle \to |e\rangle$ does not happen. The probe beam is therefore absorbed less and we see a very narrow spike in the transmission. The shape of the EIT peak is mostly dependent on the detuning of the probe- and control beam, $\Delta_p = \nu_p - \nu_{e,g_1}$ and $\Delta_p = \nu_c - \nu_{e,g_2}$. They can be chosen to be non-zero $\Delta_{p,c} \neq 0$ such that a peak is still visible.

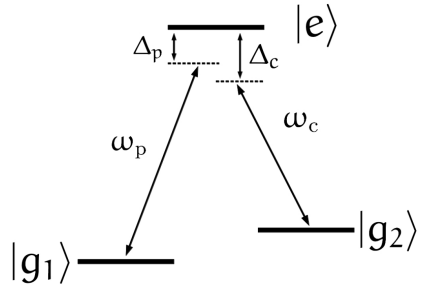

Figure 2: Schematic energy level diagram of a Λ-system with two ground states and one excited state. The probe laser couples the ground state $|g_1\rangle$ to the excited state $|e\rangle$ with the frequency $\omega_p = 2\pi\nu_p$ and the control laser couples the second ground state $|g_2\rangle$ to the excited state $|e\rangle$ with the frequency $\omega_c = 2\pi\nu_c$.

3 Setup

Component	experimented values
795 nm DFB Laser	377.10 – 377.12 THz
ND-filter	0.2, 1.0, 2.0
optical isolator	
Waveplate	$\lambda/4$, $\lambda/2$
(polarising) beam splitter	
Voltage controlled oscillators	70 – 90 MHz
Acousto- optical modulator	
Rubidium vapor chamber	28 % ^{87}Rb, 72 % ^{85}Rb, <70 °C
Copper coil (science chamber)	-5 – 5 G
Photo diodes	5 V mW^{-1}, 530 mV µW^{-1}

Table 1: List of components used in experimental setup. Where appropriate, the range in which they were operated at is given.

3.1 The Laser

We used a 795 nm semiconductor laser with a linewidth of some MHz and a maximal power output

of 80 mW. Its exact frequency is dependent on the current which is applied to it. An AF input allows us to apply an oscillating voltage to the laser current, and thereby periodically modulating the frequency of the laser beam. Using a lock box we can precisely adjust the offset and amplitude of the modulation signal.

3.2 Probe and Control Beams

A schematic of the finished setup can be seen in figure (3a). The laser beam starts off with a frequency of ω_L and then gets split into two using two polarizing beamsplitters. A waveplate before the first beamsplitter allows us to adjust how much power goes to each beam. Both then pass through an acousto-optical modulator (AOM) twice, with frequencies ω_p and ω_c respectively. Afterwards, the probe and control beams therefore have frequencies of $\omega_L + 2\omega_p$ and $\omega_L + 2\omega_c$.

The signals to the AOMs are provided by two voltage controlled oscillators (VCOs). The frequencies ω_p and ω_c of the signals are dependent on the input voltages to the VCOs. The voltage for the control beam VCO was mostly held constant throughout the experiments, such that $\omega_c \approx 80\,\text{MHz}$. The probe beam VCO was controlled by a signal generator periodically sweeping through a frequency range of $75\,\text{MHz} \leq \omega_p \leq 85\,\text{MHz}$. Note that the angle at which the first order beam exits the AOM changes with varying frequency. We therefore used a lens with a focal length of 150 mm, which parallelized all exit beams. This allowed us to reflect the beam and send it back through the AOM no matter the frequency supplied to it.

3.3 Spectroscopy setup

The spectroscopy is performed on a vapor cell filled with natural rubidium. It is an isotopic mixture of 28 % ^{87}Rb and 72 % ^{85}Rb. We take the control beam and split it into a (spectroscopy) probe beam[1] and a pump beam using a 50/50 beam splitter. The two beams are then pointed at the vapor chamber from opposite directions as shown in figure (3b). A photo diode then measures the intensity of only the (spectroscopy) probe beam.

3.4 EIT setup

For the EIT setup we take both the probe- and control beam and circularly polarize them in orthogonal directions with $\lambda/4$ waveplates. Afterwards they are superposed and sent through the science chamber. The science chamber consists of a vapor chamber filled with natural rubidium, surrounded by a copper coil and heating electronics. The coil exposes the rubidium to a magnetic field on the order of up to ± 5 Gauss ($\pm 5 \cdot 10^{-4}$ Tesla). Using a temperature probe we ensured that the vapor chamber was held at around 55 °C to 60 °C. After the two beams exit the science chamber they are again separated with $\lambda/4$ waveplates and a polarizing beamsplitter. Finally, the probe beam is measured with a more sensitive photo diode which outputs $530\,\text{mV}\,\mu\text{W}^{-1}$.

4 Experiments

4.1 Laser characterization

Firstly, we measured the intensity of the beam as a function of the current supplied to the laser. For this we simply pointed the laser along with its beam shaping elements directly at a photo diode, which output $5\,\text{V}\,\text{mW}^{-1}$. As the diode saturated at around 1.8 mW, we used a neutral density (ND) filter to measure higher intensities. An ND-filter with optical density $d = 2$ reduces the intensity by a factor of $10^d = 100$, which allowed us to measure up to the laser's rated maximum power of 80 mW at around 140 mA.

4.2 VCO Calibration

Next, we calibrated the two VCOs for the probe- and control beam. With a frequency counter we measured the frequency of the output signal for various voltages ranging from 5 V up to 12 V.

4.3 Dopplerfree spectroscopy

After setting up and properly aligning the spectroscopy setup, we heated up the rubidium vapor chamber up to a maximum of 70 °C. As we did not have a temperature probe on the spectroscopy probe, the exact temperature was unknown. By modulating the current supplied to the laser with a sawtooth wave from a signal generator, we rapidly varied the frequency of the beam. In order to see the dips from the absorption lines in the transmission signal we had to find appropriate amplitude- and offset values for the modulation signal. Once the rubidium D_1 transition spectrum was clearly visible, we took two measurements. Once with the pump beam, such that the peaks from the Doppler-free spectroscopy were visible, and once with the pump beam blocked. Each

[1] Not to be confused with the probe beam set up in the previous section.

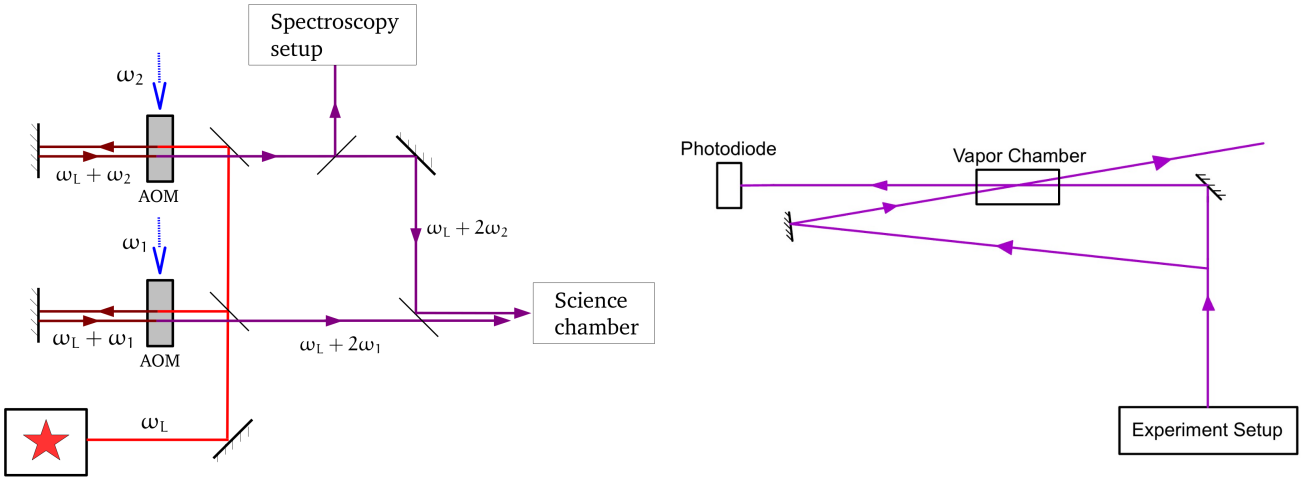

(a) complete setup

(b) spectroscopy setup.

Figure 3: Schematic overviews of (a) the complete setup and (b) the spectroscopy setup.

measurement was taken as an average over 256 samples.

4.4 Observing EIT

To observe the EIT, we first had to turn to the spectroscopy setup to set the laser frequency to around a transition frequency. We did this by adjusting and slowly decreasing the modulation signal amplitude until it was constant. Now by adjusting the sawtooth signal supplied to the probe VCO we could vary the probe beam frequency range, until the EIT peak was visible. With the peak visible, we could begin varying parameters and taking measurements.

Firstly, we exposed the rubidium vapor chamber to various magnetic fields ranging from -5G to 5G. We recorded the transmission signal for 5 different magnetic field strengths along with the signal sent to the probe VCO. This allowed us to determine the precise frequency of the probe beam.

Secondly, we turned off the magnetic field, and varied the control beam frequency. This allowed us to observe the change in shape of the EIT peak depending on the detuning of the λ-system.

For every measurement we also took a background measurement with the control beam blocked. Each measurement was again taken as an average over 256 samples.

5 Results

5.1 Laser characterization

The laser characterization measurements, shown in figure (4), revealed that the diode starts lasing at around $(48.2 \pm 1.6)\,\mathrm{mA}$. After that, the power P increased linearly with the current I:

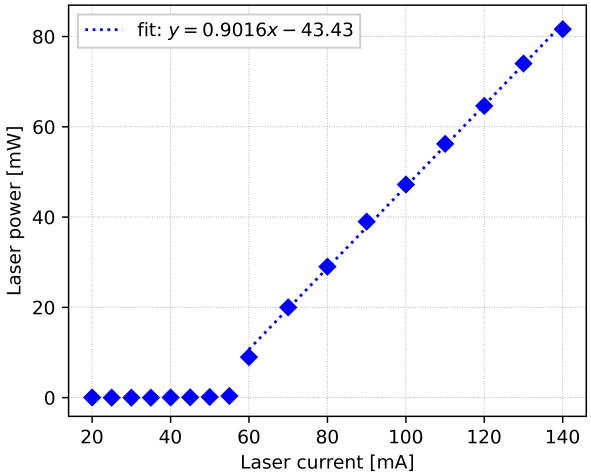

Figure 4: Laser power measured by a photo diode plotted against the current supplied to the laser. Measurement errors are smaller than the markers.

$$P(I) = (0.902 \pm 0.013)\,\frac{\mathrm{W}}{\mathrm{A}} \cdot I - (43.4 \pm 1.3)\,\mathrm{mW}$$

5.2 VCO Calibration

The output frequency of the VCOs scaled linearly with their input voltage. As can be seen in figure (5), the probe and control VCOs both behaved very similarly. The calibration fits are as follows:

$$\nu_p(U) = (4.56 \pm 0.02)\,\frac{\mathrm{MHz}}{\mathrm{V}} \cdot U + (42.5 \pm 0.1)\,\mathrm{MHz}$$
$$\nu_c(U) = (4.47 \pm 0.05)\,\frac{\mathrm{MHz}}{\mathrm{V}} \cdot U + (41.8 \pm 0.4)\,\mathrm{MHz}$$

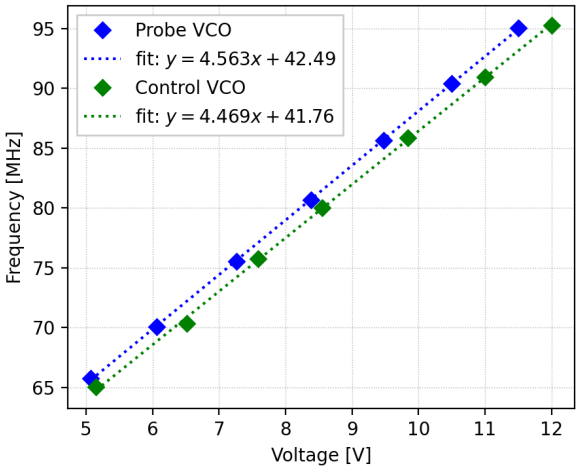

Figure 5: Calibration measurements of the probe- and control VCO. Note that they both behave very similarly. Measurement errors are smaller than the markers.

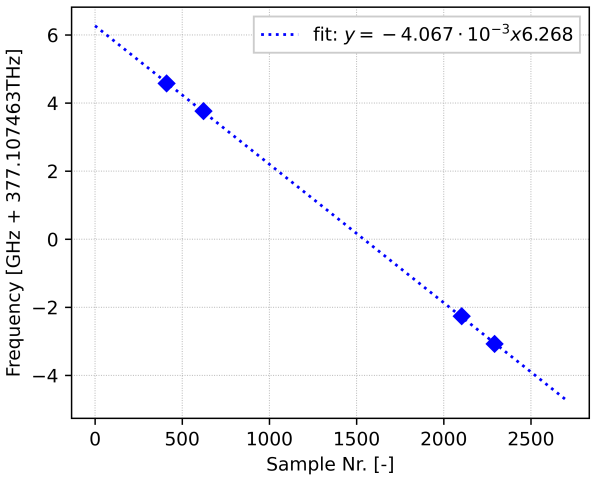

Figure 6: The four transition frequencies of ^{87}Rb as a function of the sample number of our measurements shown in figure (9a). The fit on these points is used to show the frequency on the x-axes in figure (9).

5.3 Dopplerfree Spectroscopy

Figure (9) shows our measurements of the Dopplerfree spectroscopy. In the full spectrum (9a) we see all peaks associated with the D_1 transition of ^{87}Rb and ^{85}Rb. Using the known transition frequencies of these peaks, we can fit the laser frequency onto the horizontal axis. The fit can be seen in figure (6). Figures (9b) and (9c) show finer measurements of the higher and lower energy transitions respectively. In these one can also identify the crossover resonance peak in the middle of the two ^{87}Rb transitions.

We can estimate the temperature of the vapor chamber by fitting the Doppler broadened dips with a Gaussian to get the FWHM and finally calculate T using (2). Because we vary the laser beam frequency by varying its supply current, which also changes the beam intensity, the transmission slightly increases linearly with the frequency. We therefore add a linear term to the Gaussian:

$$P(\nu) = a \exp\left(-\frac{(x-p)^2}{2w^2}\right) + sx + o. \qquad (3)$$

In figures (9b) and (9c) we fit the parameters a, p, w, s and o of (3) to the $F = 2 \to F = 1$ and the $F = 1 \to F = 2$ transitions. The full width at half maximum is then given by $\text{FWHM} = 2\sqrt{2\ln 2} \cdot w$. We calculated the following temperatures:

	FWHM	T
$F = 1 \to F = 2$:	(538 ± 5) MHz	$(72 \pm 6)\,^\circ$C
$F = 2 \to F = 1$:	(514 ± 3) MHz	$(42 \pm 4)\,^\circ$C

5.4 EIT

We were able to observe and take measurements for three of the four D_1 transitions of ^{87}Rb. These can be seen in figures (10a), (10c) and (10e) for various magnetic field strengths. Note that even though the background transmission is subtracted in these plots, the peaks still look very noisy and are shifted vertically for different B-field strengths.

Figures (10b), (10d) and (10f) plot the difference of the probe- and control beam frequency at the EIT peaks $\Delta\nu = \nu_p - \nu_c$ against the magnetic field strengths. We expect $\Delta\nu$ to be exactly equal to energy splitting due to the Zeeman effect $\Delta Z = \Delta E/h$, as given by (1). With the Lande factor $g = 1/2$ and the difference in the magnetic quantum number $\Delta m_F = 2$, we predict

$$\Delta Z(B) = 1.399\,624\,493\,61\,\text{MHz/G} \cdot B.$$

The slope indeed corresponds with our measurements:

	Slope
$F = 1 \to F = 1$:	(-1.258 ± 0.017) MHz/G
$F = 2 \to F = 2$:	(1.423 ± 0.096) MHz/G
$F = 2 \to F = 1$:	(1.385 ± 0.011) MHz/G

Though, we see a small offset of about

$$\delta B = (0.46 \pm 0.21)\,\text{G} = (46 \pm 21)\,\mu\text{T}.$$

This coincides very nicely with the typical value of the earths magnetic field, which in Zurich is around 48 µT[1].

[1] www.magnetic-declination.com

Finally, in figure (7) we see the shape of the EIT peak for various detunings of the control beam frequency. The magnetic field is turned off, so we expect the center of the peaks to be at $\Delta\nu = 0\,\text{MHz}$, which is exactly what we see. Figure (8) show the EIT peak heights as a function of the detuning.

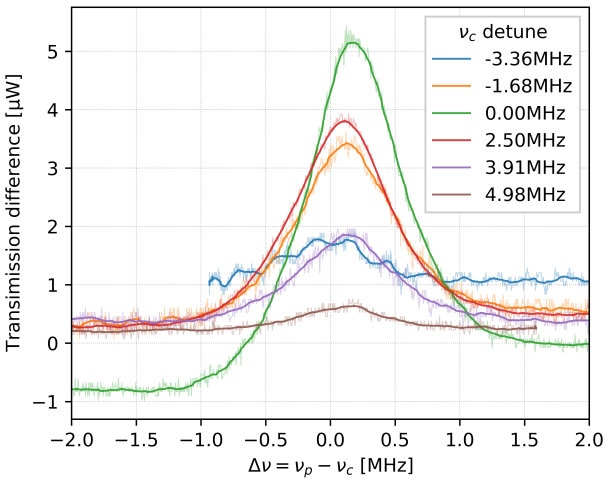

Figure 7: EIT peak of the ^{87}Rb, D_1, $F = 1 \rightarrow F = 2$ transition for various control frequency detunings and no magnetic field. Note that 0.00 MHz detuning was chosen as the value of ν_c where the peak was largest. A 32-frame moving average is shown above the raw data for each measurement.

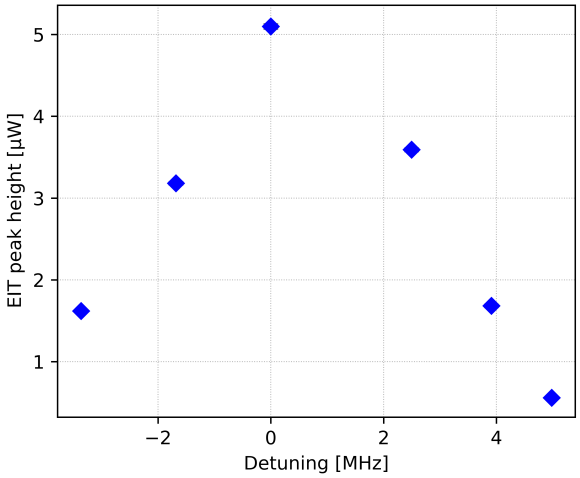

Figure 8: The EIT peak height from figure (7) as a function of the detuning. We see the height decreases symmetrically with positive and negative detuning.

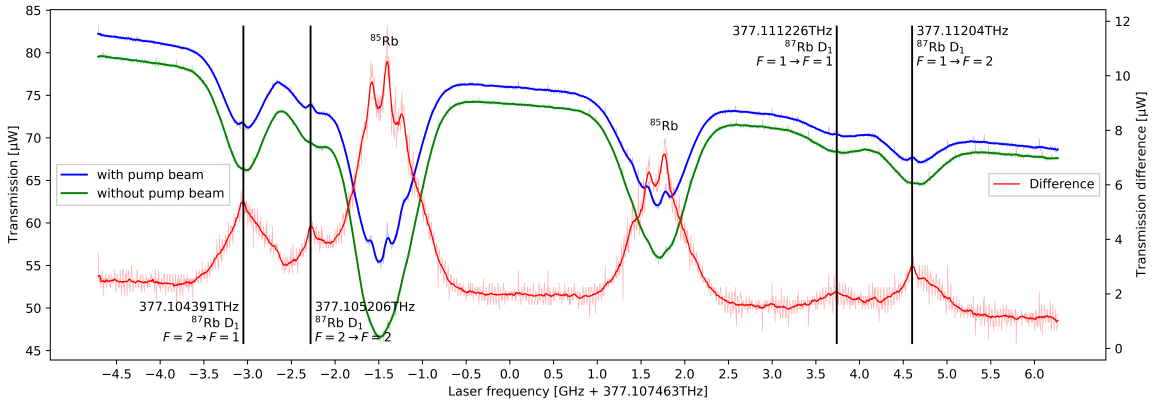

(a) full Rubidium spectrum

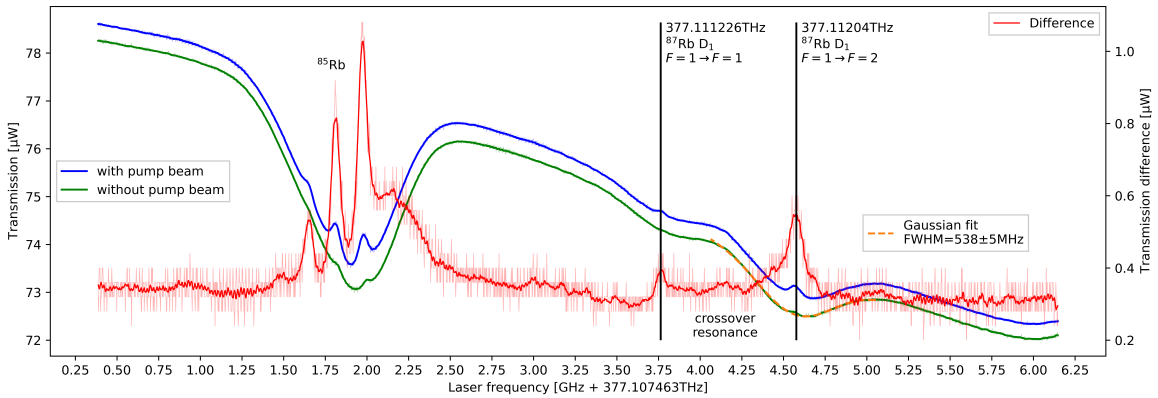

(b) higher energy transitions

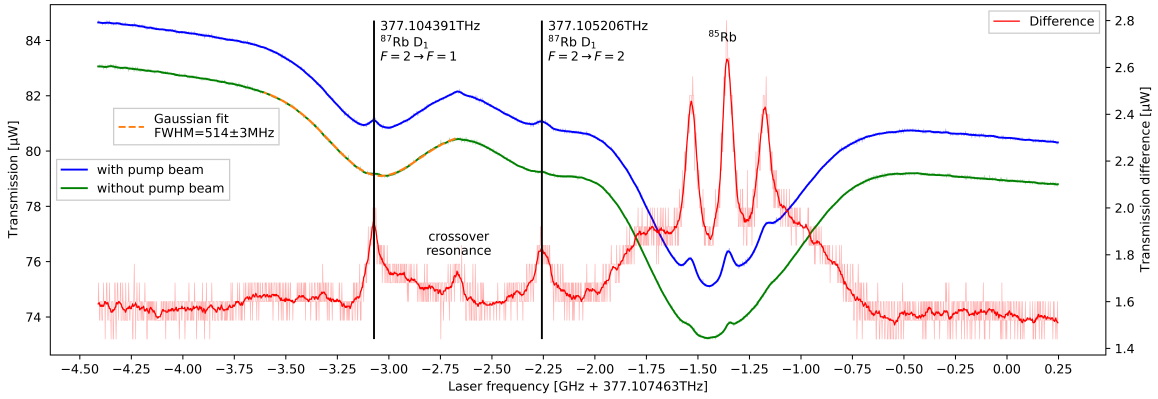

(c) lower energy transitions

Figure 9: Spectroscopy measurements of (a) the full spectrum and two finer measurements (b) and (c). The green line shows the transmission of the probe beam without the pump beam and the blue line with the pump beam. The red line is their difference. For all of them the 16-frame moving average is shown above the raw data.

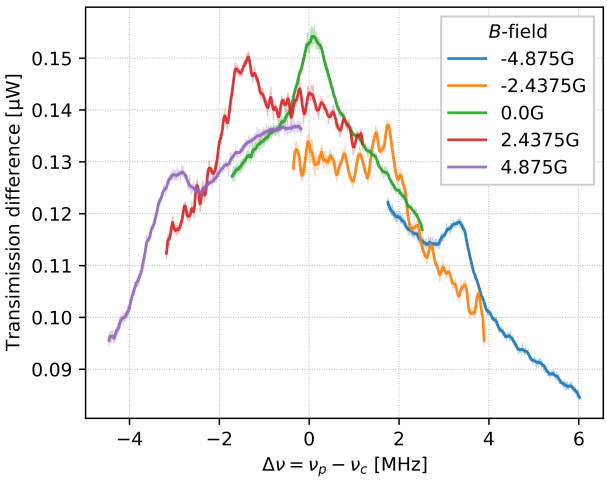

(a) ^{87}Rb, D_1, $F = 1 \rightarrow F = 1$

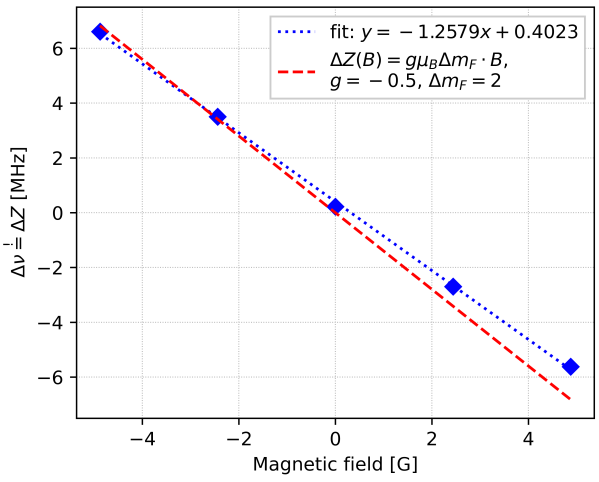

(b) ^{87}Rb, D_1, $F = 1 \rightarrow F = 1$

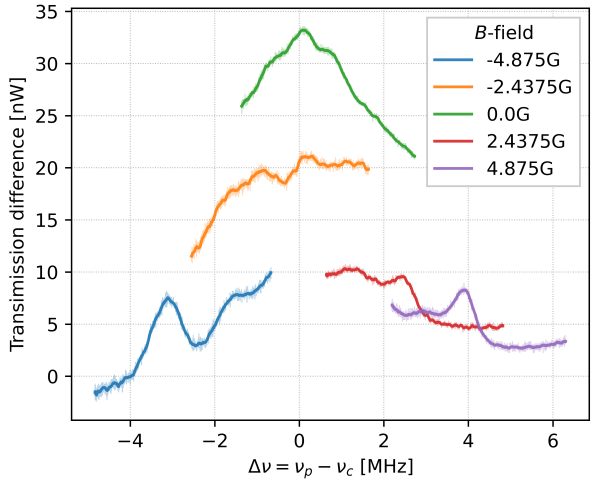

(c) ^{87}Rb, D_1, $F = 2 \rightarrow F = 2$

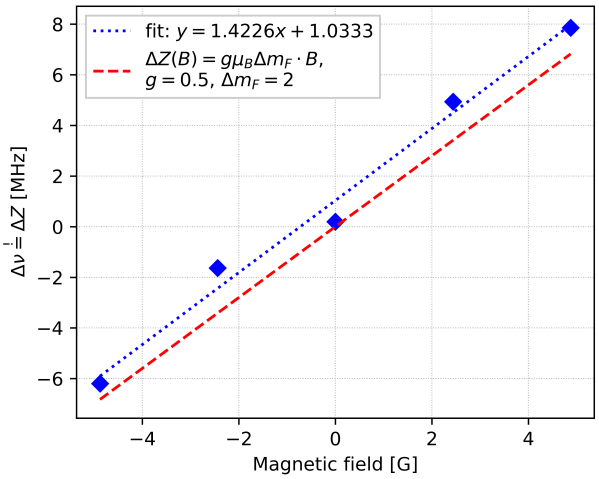

(d) ^{87}Rb, D_1, $F = 2 \rightarrow F = 2$

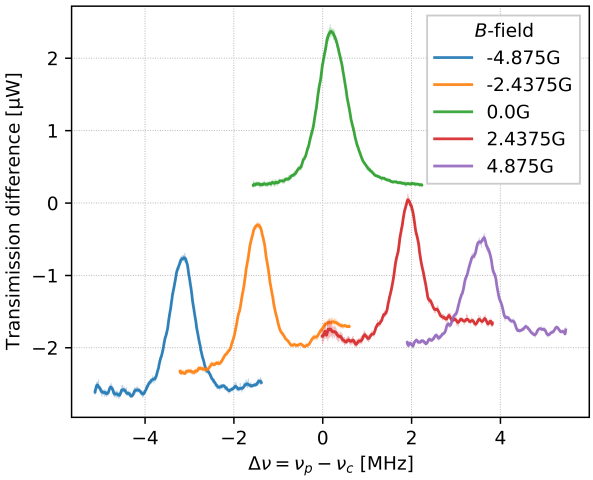

(e) ^{87}Rb, D_1, $F = 2 \rightarrow F = 1$

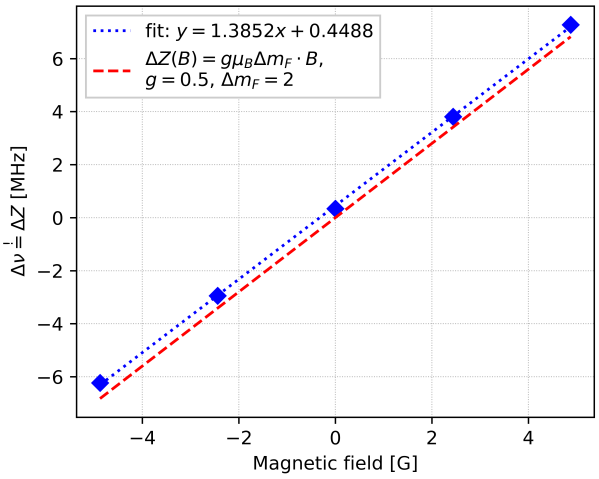

(f) ^{87}Rb, D_1, $F = 2 \rightarrow F = 1$

Figure 10: *Left column:* Transmission signal with background signal (blocked control beam) subtracted, plotted against the frequency difference $\Delta\nu = \nu_p - \nu_c$ of the probe and control beam, for various magnetic field strengths. A 32-frame moving average is shown above the raw data. *Right column:* The frequency difference $\Delta\nu = \nu_p - \nu_c$ of the control and probe beam at the EIT peaks as a function of the magnetic field strength. $\Delta\nu$ should be equal to the Zeeman energy splitting $\Delta Z = \Delta E/h$ of the ground states, as given in (1). The red dashed line shows the theoretical prediction.

6 Discussion

6.1 Dopplerfree Spectroscopy

The absorption spectrum that we managed to measure, shown in figure (9), ended up very good. We could clearly identify all the absorption lines and crossover resonance peaks. The lower energy transitions were definitely more prominent though, possibly due to the fact that our beam lases at a higher intensity for lower frequencies.

The temperatures that we calculated from the Doppler broadening also turned out reasonable. As we had no sensor to measure the temperature we simply let the vapor chamber heat up until the absorption dips were visible, while being careful not to overheat it. The temperature for the lower energy transition turned out to be much lower, which again can be explained by the fact that our beam had greater intensity for lower frequencies. As the dips were already visible for lower temperatures, we did not feel the need to increase the temperature.

6.2 EIT

We managed to measure the EIT peak for all transitions except for the ^{87}Rb, D_1, $F = 1 \rightarrow F = 2$, which is the highest energy transition. The reason for this is not entirely clear, it could well be possible, that with further tweaking and optimizing we could also have measured that. The peaks belonging to the transitions $F = 1 \rightarrow F = 1$ and $F = 2 \rightarrow F = 2$ were also not incredibly clear. The vertical shifts for the peaks of various B fields can be attributed to small temperature changes between the measurements with the control beam and those without. But this should not have affected the overall shape of the signal significantly.

The best results were yielded by the $F = 2 \rightarrow F = 1$ transition. This also gave us the best agreement with the theory in figure (10e). The displacements in the other two graphs can be explained by the noisy peaks, which made it harder to identify their center. Over all measurements in figure (10), we measured an average $\Delta Z(B)$ slope of $(1.344 \pm 0.032)\,\mathrm{MHz/G}$, which is within 96.8 % of the theoretical value.

Finally, the shape of the EIT peak also behaved as expected for various detunings. Notice how the peaks for two roughly equal, but opposite detunings have very similar shapes.

7 Conclusion

We built a setup with various optical components, that simultaneously performs Doppler-free absorption spectroscopy on a rubidium vapor chamber and that allowed us to observe an electromagnetically induced transparency. This effect is due quantum interferences in three-state systems. Here, we created several Λ-systems with two ground states and one excited state, by placing the rubidium probe inside of a magnetic field. The Zeeman splitting then allowed us to excite certain transitions with appropriately circularized light.

After we optimized the setup, we managed to obtain mostly very clear measurements of the effects we were looking for. Namely the Absorption spectra in figure (9) and the EIT peaks in figure (10). From the Doppler broadened dips in the spectograms we determined the temperature of the probe to have been $(72 \pm 6)\,^\circ\mathrm{C}$ and $(42 \pm 4)\,^\circ\mathrm{C}$ in the two measurements that we took. Further, the offset in the magnetic field measurements roughly coincides with the earths magnetic field of 48 µT and other parasitic magnetic fields. The slope in the magnetic filed measurements was calculated to be $(1.344 \pm 0.032)\,\mathrm{MHz/G}$, which is within 96.8 % of the theoretical value. Finally, we briefly looked at the shape of the EIT peak depending on the detuning of the control beam frequency, as shown in figure (7). Here we also found, that it behaved as expected.

References

[1] Rafael Mottl (October 2014, Version 1.1) *Atom-Photon Interaction*, ETH Zurich.

[2] D. A. Steck (2010, revision 2.1.4) *Rubidium 87 D Line Data*, http://steck.us/alkalidata.

[3] D. A. Steck (2010, revision 2.1.4) *Rubidium 85 D Line Data*, http://steck.us/alkalidata.

[4] Michael Fleischhauer, Atac Imamoglu, Jonathan P. Marangos (12 July 2005) *Electromagnetically induced transparency: Optics in coherent media*, Reviews of Modern Physics, Volume 77, April 2005.